Discover Oncology

Research

Identification of benign from malignant small renal tumors: is there a possible role of T1 mapping?

Lianting Zhong[1] · Danlan Lian[1] · Ying Zhang[2] · Yuqin Ding[3,4] · Shengxiang Rao[3,4,5] · Jiefeng Guo[6,7] · Weifeng Lin[8] · Xiaobo Qu[7,9] · Jianjun Zhou[1,10,11,12]

Received: 12 January 2025 / Accepted: 7 May 2025
Published online: 19 May 2025

Abstract

Purpose Differentiating benign from malignant small renal tumors (SRMs) can help to guide clinical decision-making. T1 mapping enables quantitative assessment of T1 relaxation time and may help to evaluate SRMs properties. This study aimed to investigate the possible utility of T1 mapping for identification of SRMs.

Methods The data set used in this retrospective study, consisted of 104 patients with SRMs (≤ 4 cm). 78 malignant and 25 benign ones respectively. Calculated and compared the quantitative variables (including T1 mapping) between different renal tumors. The clinical features qualitative characteristics were subsequently documented. Finally, the logistic regression models were used to identify independent influencing factors. The diagnostic accuracy of independent influencing factors was represented with the area under the receiver operating characteristic curve (AUC).

Results The pre-contrast T1 mapping (T1) and the ratio of T1 reduction in malignance were higher than those in benign SRMs, while post-contrast T1 mapping was lower (all $P < 0.025$). In multivariable logistic regression, the tumor necrosis (odds ratio (OR) = 20.636, $P = 0.005$) and T1 (OR = 2.982, $P = 0.002$) were independent predictors. For the identification of SRMs, the performance of the model achieving an AUC of 0.793 (95% CI 0.701–0.866) when combining two factors.

Conclusion Quantitative T1 mapping parameters may be a new potential biomarker for noninvasively distinguishing SRMs.

Keywords Magnetic resonance imaging · Identify · Renal neoplasm

✉ Xiaobo Qu, quxiaobo@xmu.edu.cn; ✉ Jianjun Zhou, zhoujianjunzs@126.com | [1]Department of Radiology, Zhongshan Hospital (Xiamen), Fudan University, 668 Jinhu Road, Huli District, Xiamen 361015, China. [2]Department of Nuclear Medicine, Zhongshan Hospital (Xiamen), Fudan University, Xiamen 361015, China. [3]Department of Radiology, Zhongshan Hospital, Fudan University, Shanghai 200032, China. [4]Shanghai Institute of Medical Imaging, Shanghai 200032, China. [5]Cancer Center, Zhongshan Hospital, Fudan University, Shanghai 200032, China. [6]Department of Microelectronics and Integrated Circuit, Xiamen University, Xiamen 361102, China. [7]Fujian Provincial Key Laboratory of Plasma and Magnetic Resonance, Xiamen University, Xiamen 361102, China. [8]Department of Information, Zhongshan Hospital (Xiamen), Fudan University, Xiamen 361015, China. [9]Department of Electronic Science, Xiamen University, Xiamen 361102, China. [10]Xiamen Municipal Clinical Research Center for Medical Imaging, Xiamen 361015, China. [11]Fujian Province Key Clinical Specialty for Medical Imaging, Xiamen 361015, China. [12]Xiamen Key Laboratory of Clinical Transformation of Imaging Big Data and Artificial Intelligence, Xiamen 361015, China.

1 Introduction

The incidence of diagnosed solid renal masses has been increasing rapidly in the past few decades, due to the widespread utilization of cross-sectional imaging [1]. However, there has not been an obvious decrease in kidney cancer-specific mortality with the increased number of surgeries and ablations performed for suspected renal masses [2–4]. While mostly incidentally found solid renal masses are notorious renal cell carcinomas (RCC), the benign tumors account for 20% of excised small (< 4 cm) solid renal masses (SRMs) [5, 6]. Active surveillance is supported by evidence that many benign masses are resected unnecessarily [7, 8]. To decrease patient morbidity and healthcare costs related to unnecessary surgery treatments, the discrimination of suspicious SRMs before surgery is crucial for the appropriate treatment planning [9, 10].

The percutaneous biopsy has been proposed [11] for diagnosing benign and malignant, but the invasiveness and complications cannot be ignored [12–14]. Besides, the percutaneous biopsy was not suitable for every patient, especially elderly individuals with multiple underlying conditions [15, 16]. MRI has an excellent soft-tissue contrast, predominant noninvasive methodologies used in the diagnosis of renal masses [17]. Due to morphological, non-quantitative features and substantial overlap between benign and malignant small renal masses on conventional MRI, radiologists are facing enormous challenges [18, 19]. Thus, more diagnostic information is expected to be provided.

Longitudinal relaxation time (T1) was a property determined by a tissue's molecular composition that is related to water content and mobility. T1 mapping can provide quantitative information about longitudinal relaxation time at each pixel. In renal MRI, measuring the T1 relaxation time of water molecules may present a valuable biomarker for a variety of pathological mechanisms [20]. Lisa showed that T1 mapping allowed for a noninvasive quantification of the extracellular volume fraction of renal tumors [21]. Previous studies demonstrated that the T1 mapping was feasible for evaluating the severity of fibrosis or inflammation changes in nephropathy [22–24], predicting the histopathological grade of clear cell renal cell carcinoma (ccRCC) [21], and distinguishing ccRCC from fat-poor angiomyolipoma [25]. However, the efficacy of T1 mapping for the discrimination of SRMs is entirely unexplored.

This study aimed to evaluate if the quantitative T1 mapping can be used as a preoperative predictor of benign SRMs, which would be particularly helpful for clinical decisions.

2 Methods and methods

2.1 Patients

The study was conducted in accordance with the Declaration of Helsinki. We obtained permission from The Ethics Committee of Fudan University Affiliated Zhongshan Hospital (No. B2020-214R). Informed consent requirement was waived because of its retrospective nature. We reviewed surgical resected SRMs between September 2014 and September 2021 from our Hospital. All patients performed magnetic resonance imaging (MRI) scanning within 1 month before resection for clinical diagnosis. Exclusion criteria are as follows: (a) patients receiving preoperative neoadjuvant therapy; (b) poor imaging quality (e.g., obvious motion artifacts and blurred blood vessels) or incomplete scan protocol (e.g. without T1 mapping); and (c) pathologically proven renal cysts or classical angiomyolipoma. Figure 1 shows an overview of the study workflow.

2.2 MRI protocols

All patients with renal lesions were scanned with the same 1.5 T MRI system (Magnetom Area; Siemens Healthineers) using an 18-channel body array coil. Conventional renal MRI includes: (1) axial T1-weighted in-and-out-of-phase imaging with volume interpolated breath-hold examination (VIBE); (2) axial T2-weighted imaging with fat suppression; and (3) fat saturation VIBE-T1-weighted imaging. The corticomedullary phase (CMP) and nephrographic phase (NP) were obtained in the 20 s and 80 s after intravenous injection of the gadopentetate dimeglumine (Magnevist; Bayer Schering Pharma AG), respectively. The T1 mapping was performed with a dual flip-angle 3D gradient-echo VIBE sequence. Pre- and post-contrast-T1 mapping images (T1 and T1e) were obtained before and after 90–120 s

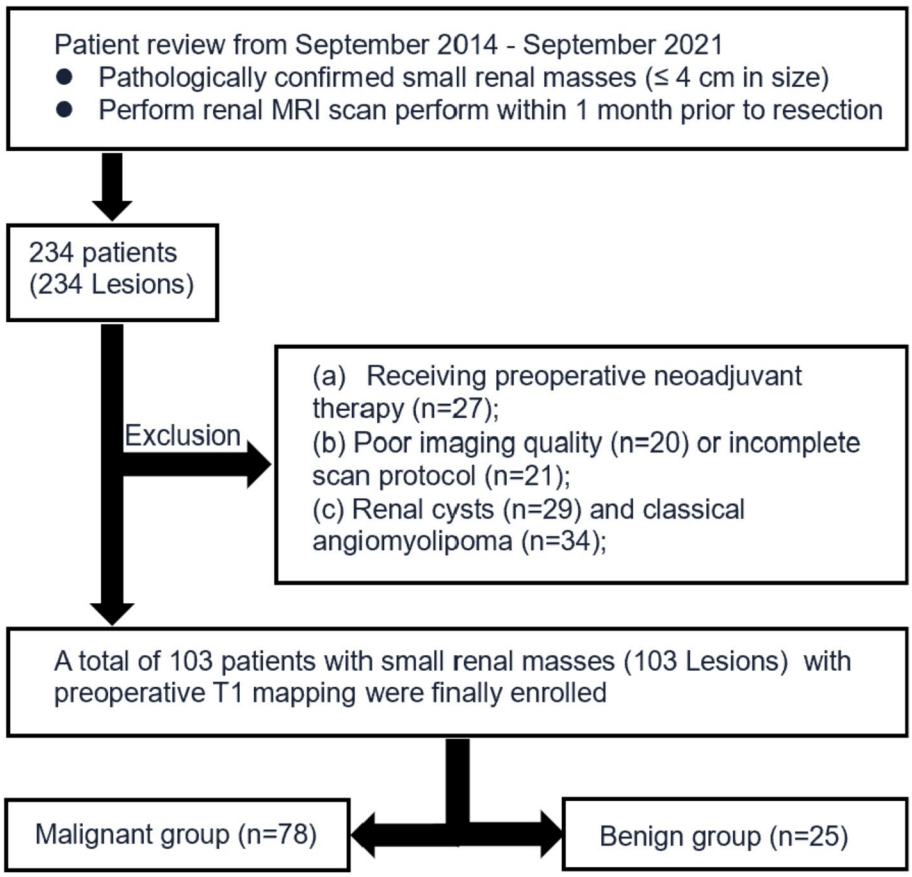

Fig. 1 Flowchart of the study population

the intravenous contrast administration respectively. The parameters were as follows: TR = 4.38 ms; TE = 1.93 ms; flip angle, 2° and 12°; FOV, 380–400 × 300–324 mm^2; matrix size, 216 × 288; slice thickness, 5 mm. All patients were injected with 0.1 mmol/kg body weight of Gd-DTPA at a rate of approximately 2 ml/s.

2.3 Quantitative MRI image analysis

All MRI images were processed at the same Syngo workstation. The regions of interest (ROI) were delineated by two observers with over 3 (ZLT) and 10 (DYQ) years of experience in diagnostic abdominal radiology respectively, neither of whom had prior knowledge of pathological data. For each tumor, an ROI was drawn on the NP sequence and it was copied to the corresponding other MRI sequence, followed by validation through review by specialized radiologists. The ROI included the solid components of the lesion and was set as large as possible. We try to minimize selection bias by avoiding renal parenchyma, perirenal fat, as well as intra-tumor heterogeneous components (such as necrosis, cystic degeneration, hemorrhage, calcification, and peritumoral membranes). In predominantly solid SRMs, the ROI would cover the whole tumor. Repeated the measurement method 3 times and the mean of 3 values was used in the analysis. Finally, the average value measured by the two observers was taken. The mean ROI area of all tumors was 82.3 mm^2 (range 56.4–160.0 mm^2). Figure 2 shows the different SRMs images and the ROI.

The enhanced ratios of CMP (CMPr) and NP (NPr) and the ratio of T1 reduction (T1r) were calculated as follows:

$$\mathrm{CMPr/NPr} = (\mathrm{CMP/NP} - \mathrm{T1WI})/\mathrm{T1WI} \times 100\%;$$

$$\mathrm{T1r} = (\mathrm{T1} - \mathrm{T1e})/\mathrm{T1} \times 100\%.$$

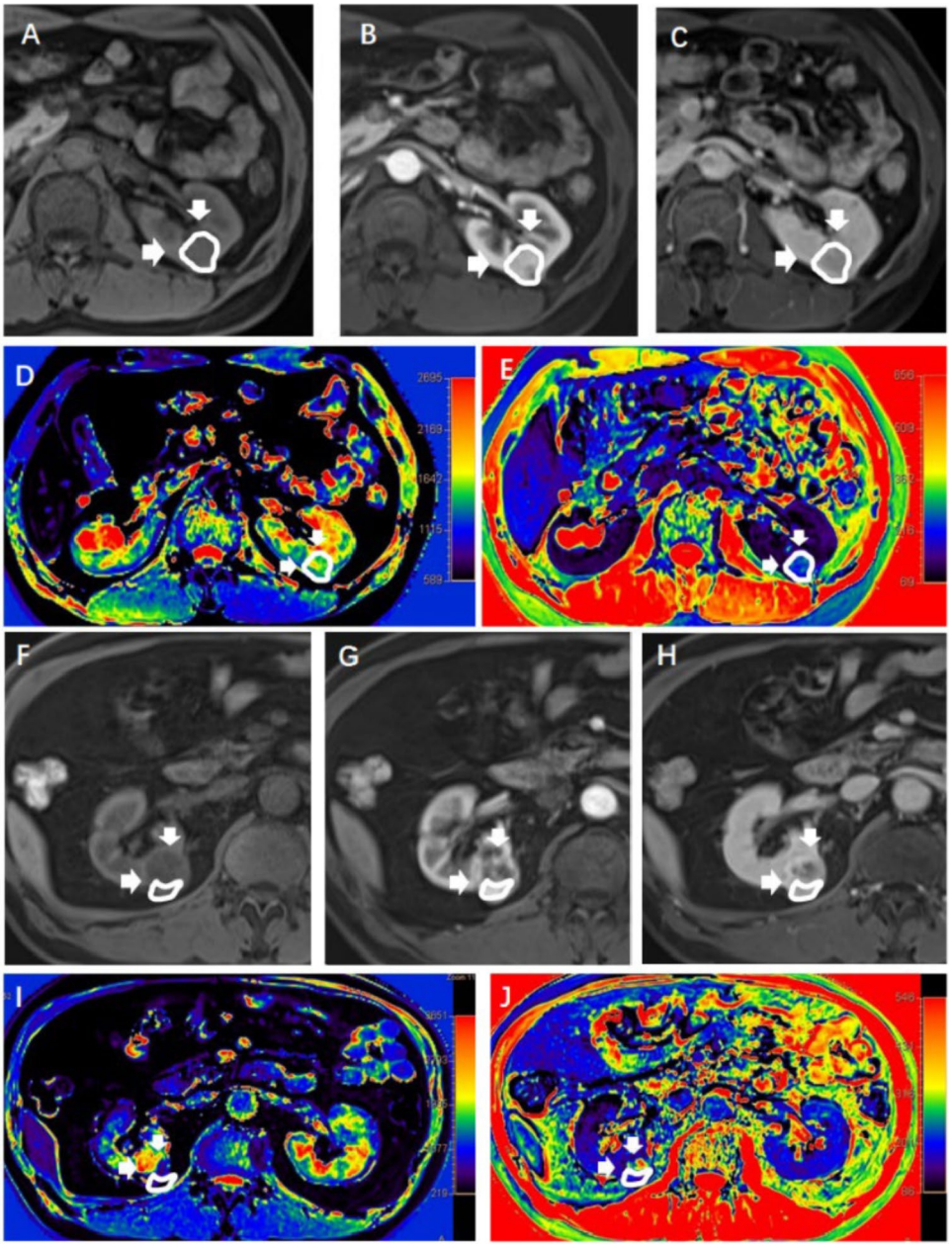

Fig. 2 MRI of different renal lesions. The lesion (ROI) demonstrates the maximum area of the solid component on the tumor at each sequence. The arrows indicate the entire tumor. A and F: T1-weighted imaging, B and G: corticomedullary phase, C and H: nephrographic phase, D and I: pre-contrasted T1 mapping, E and H: post-contrasted T1 mapping. **A**–**E** a 49-year-old man with pathologically confirmed fat-poor angiomyolipomas (AML) in the left kidney. **A** The tumor showed marginally low signal intensity on pre-contrasted T1-weighted imaging. **B** The lesion demonstrated obvious overall uniform enhancement in the corticomedullary phase and **C** hypo-intensification in the nephrographic phase. The pre-contrasted T1 mapping **D** and post-contrasted T1 mapping **E** of the lesion, with a T1 relaxation time of 1733.17 ms and 273.68 ms, respectively. **F**–**J** a 66-year-old man with pathologically confirmed papillary RCC in the right kidney. **F** The tumor showed low signal intensity on pre-contrasted T1-weighted imaging. **G** The lesion demonstrated obvious local enhancement in the corticomedullary phase and **H** hypo-intensification in the nephrographic phase. The pre-contrasted T1 mapping **I** and post-contrasted T1 mapping **J** of the lesion, with a T1 relaxation time of 2370.56.48 ms and 184.24 ms, respectively

2.4 Statistical analysis

Statistical analyses were performed with SPSS (version 26.0). The independent T-test and Mann–Whitney U test were used for quantitative analysis, and Fisher exact tests were used for qualitative analysis. Univariate and multivariate logistic regression were summarized with influence factors and 95% confidence intervals (CIs). Those factors with *P* values < 0.05 in univariate analysis were included in multivariate analysis. The receiver operating characteristic (ROC) curve analysis was used to evaluate the diagnostic efficacy of different factors, and optimal cutoff values of ROC curves were calculated from the Youden index. The DeLong nonparametric method was used to compare ROC curves. Interobserver agreement was assessed using the intraclass correlation coefficient (ICC). The grades of 0.2, 0.21–0.40, 0.41–0.60, 0.61–0.80, and 0.81–1.00 indicate the slight, fair, moderate, substantial, and perfect ICC value, respectively. *P* values less than 0.05 were considered statistically significant.

Table 1 Clinical and pathological characteristics of enrolled patients

Variables	All lesions	Malignance (n = 78)	Benign (n = 25)	*P* values
Gender				0.001
Male	65 (63%)	55 (53%)	8 (9%)	
Female	39 (36%)	23 (22%)	16 (13%)	
Mean age (years)	54.2 ± 11.0 (27–83)	55.8 ± 10.6(27–83)	49.1 ± 11.0 (29–68)	0.007
Surgery type				0.654
Partial nephrectomy	79 (76%)	59 (57%)	20 (19%)	
Radical nephrectomy	24 (23%)	19 (18%)	5 (5%)	
Mean size(cm)	2.8 ± 0.86 (1.1–4.0)	2.9 ± 0.72 (1.1–4.0)	2.8 ± 0.75 (1.2–4.0)	0.192
Tumor subtype				
Clear cell RCC	–	48 (46%)	–	
Papillary RCC	–	16 (15%)	–	
Chromophobe RCC	–	14 (13%)	–	
Angiomyolipoma	–	–	18 (17%)	
Oncocytoma	–	–	7 (7%)	

Data are numbers of patients with percentages in parentheses, or means ± standard deviation with range in parentheses

Table 2 Qualitative radiological parameters of different SRMs

Parameter	Malignant (n = 78)	Benign (n = 21)	P values
CMPr (%)	198.97 ± 131.02	173.33 ± 106.32	0.415
NPr (%)	231.82 ± 113.90	227.44 ± 102.81	0.864
T1 relaxation time			
T1 (ms)	2047.16 ± 619.21	1594.88 ± 328.60	0.001
T1e (ms)	244.42 ± 87.57	282.02 ± 42.96	0.042
T1r (%)	85.92 ± 8.71	80.93 ± 8.14	0.013

CMPr, the enhanced ratios of the corticomedullary phase; NPr, the enhanced ratios of the nephrographic phase; T1, native T1 mapping; T1e, enhanced T1 mapping; T1r, the reduced ratio of T1 mapping

3 Results

3.1 Population characteristics

A total of 104 patients included 65 males (63%) and 39 females (36%) with a mean age of 54.2 ± 11.0 years (range, 27–83 years). The mean size of small solid renal masses is 2.8 ± 0.86 cm (range, 1.1–4.0 cm). All patients were given a pathologic diagnosis after partial or radical nephrectomy. The most common tumors were clear cell RCC (n = 48), followed by papillary RCC (n = 16) and chromophobe RCC (n = 14) respectively. Benign histology included 18 minimal fat AMLs and 7 oncocytomas. The conventional clinical and pathological description of all renal masses is summarized in Table 1.

3.2 Qualitative radiological parameters

The qualitative parameters of SRMs are shown in Table 2. The T1 and T1r of benign renal tumors were lower than those of malignant ones ($P = 0.001$ and $P = 0.013$, respectively), while the T1e was higher ($P = 0.042$). However, the difference in CMPr and NPr values between benign and malignant renal tumors was not statistically significant ($P > 0.05$). Bland–Altman shows a small difference in the T1 mapping parameters between benign and malignant lesions (Fig. 3).

The interobserver agreement of the quantitative features were good, with mean of ICC 0.964 (95% CI 0.947–0.975) for assessment the CMPr, 0.910 ((95% CI 0.869–0.938) for the NPr, 0.912 (95% CI 0.872–0.939) for the T1, 0.828 (95%

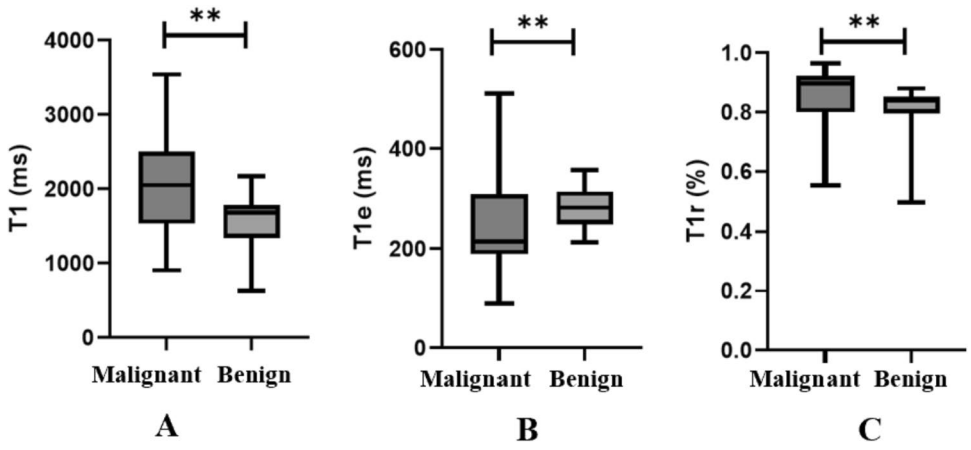

Fig. 3 Each box clarified the small difference in T1, T1e, and T1r between benign and malignant lesions. Box shows the mean values and 25 th, 50 th, and 75 th percentiles. Vertical bars showed the ranges of data that were not outliers. ** means the statistical significance between the two groups, $P < 0.05$. A. T1, native T1 mapping; B.T1e, enhanced T1 mapping; C. T1r, the reduced ratio of T1 mapping

Table 3 Parameters of each small renal tumor for different observers

Parameter	Observer 1	Observer 2	ICC (95% CI)
CMPr (%)	193.23 ± 125.39	202.39 ± 114.83	0.964 (0.947–0.975)
NPr (%)	230.76 ± 110.83	244.85 ± 99.04	0.910 (0.869–0.938)
T1 relaxation time			
T1(ms)	1950.45 ± 573.33	1924.12 ± 639.95	0.912 (0.872–0.939)
T1e(ms)	257.39 ± 83.30	249.70 ± 85.14	0.828 (0.757–0.881)
T1r(%)	81.64 ± 18.24	81.02 ± 19.06	0.973 (0.961–0.982)

ICC, intraclass correlation coefficient

CI 0.757–0.881) for the T1e, 0.973 (95% CI 0.961–0.982) for the T1r, respectively. The agreement between observers for the quantitative value is shown in Table 3.

3.3 Independent parameters for characterizing small renal neoplasms

Results from logistic regression analysis are shown in Table 4. At univariate logistic regression analysis, the no-tumor necrosis, angular interface, T2 hypointense, ADC hyperintense, the higher post-contrasted T1 relaxation time, the lower pre-contrast T1 and the ratio of T1 reduction were statistically correlated to the small benign renal tumor. Multivariable logistic regression revealed that the tumor necrosis (OR 20.636, 95% CI 2.490–171.000, $P = 0.005$), and pre-contrast T1 relaxation time (OR 2.982, 95% CI 1.479–6.015, $P = 0.002$) were independently predictive of malignant renal tumors from benign ones.

3.4 ROC curves analyze the diagnostic value of T1 mapping

ROC curves of independent characteristics for predicting benign renal tumors were plotted in Fig. 4. The AUC for distinguishing benign from malignant SRMs using the T1 was 0.692 (95% CI 0.594–0.780), with 2186.2 ms as the optimal diagnostic threshold; the diagnostic sensitivity and specificity were 47.44% and 100%, respectively. The renal tumor necrosis achieved an AUC of 0.685 (95% CI 0.586–0.773), a sensitivity of 41.03%, a specificity of 96.00%. The T1 + tumor necrosis model achieved an AUC of 0.792 (95% CI 0.701–0.866), a sensitivity of 69.23%, a specificity of 96.00%.

4 Discussion

Preoperative differentiation between benign and malignant small renal masses enables rational therapeutic decision-making, and reducing the risk of unnecessary invasive interventions [26]. In this study, we developed a binary logistic regression model. The result demonstrated that the pre-enhanced T1 relaxation time and tumor necrosis

Table 4 Univariate and multivariate Logistic regression analyses of malignant and benign renal tumors

Variable	Univariate analysis		Multivariate analysis	
	OR (95%CI)	P	OR (95%CI)	P
Mean size (cm)	1.150(0.632–2.092)	0.648		
Growth pattern				
Exophytic	Reference	0.070		
Mixed	0.500(0.154–1.619)	0.248		
Endophytic	1.833(0.468–7.187)	0.385		
Shape (round/irregular)	0.612(0.217–1.730)	0.355		
Necrosis (Y: N)	16.696(2.148–129.772)	0.007*	20.636(2.490–171.000)	0.005*
Hemorrhage (Y: N)	0.875(0.280–2.730)	0.818		
Cystic (Y: N)	2.612(1.046–6.521)	0.040		
Central scar (Y: N)	0.723(0.172–3.035)	0.658		
Angular interface (Y: N)	0.160(0.035–0.727)	0.018*		
Segmental enhancement (Y: N)	0.502(0.111–2.271)	0.371		
T2 signal (Hyper-/Hypointense)	3.694(1.332–10.246)	0.012*		
ADC signal (low/no)	0.341(0.116–1.002)	0.050*		
Out-of-phase T1 (Signal dropout/No)	1.190(0.456–3.106)	0.722		
Strengthen degree				
Low	Reference	0.377		
Middle	0.471(0.156–1.419)	0.181		
High	1.029(0.294–3.598)	0.964		
Strengthen formal				
Wash-in and wash-out	Reference	0.177		
Persistent enhancement	4.560(0.910–22.845)	0.065		
Delay enhancement	1.484(0.564–3.904)	0.424		
CMPr	1.224(0.756–1.982)	0.412		
NPr	1.041(0.660–1.643)	0.863		
T1 relaxation time				
T1(ms)	2.624 (1.430–4.812)	0.002*	2.982(1.479–6.015)	0.002*
T1e(ms)	0.628(0.397–0.993)	0.047*		
T1r(%)	1.714(1.092–2.692)	0.019*		

Data in parentheses are 95% CI

Each variable with $P < 0.05$ at univariate analysis was entered into the multivariate analysis

The * means $P \leq 0.05$

were independent predictors for the identification of benign small renal tumors, achieving an AUC of 0.793 (95% CI 0.701–0.866) when combining two factors.

What could be the potential explanation for the efficacy of pre-enhanced T1 mapping in the detection of benign renal tumors in our study? It may be explained by the following reasons. Firstly, malignant renal tumors are always more heterogeneous than benign tumors, exhibit higher levels of necrosis, and are more likely to contain cysts. Although we have avoided these areas in our ROIs, it may still be difficult to totally exclude macroscopic zones [27]. Secondly, the upregulation of genes and proteins within the extracellular matrix could play a significant role in malignant renal tumors. It is common for poorly differentiated renal tumors to exhibit irregular tumor cells and loose intercellular spaces [21]. In contrast, fp-AML is characterized by spindle cells or epithelioid smooth muscle cells with abnormal thick-walled blood vessels in variable proportions, which would indicate tiny intercellular spaces. This may demonstrate a benign renal tumor with a lower T1 relaxation time [21, 28].

An interesting observation is that the native T1 mapping was an independent influence factor for diagnosing benign renal tumors, but the enhanced T1 mapping was not. In general, enhanced T1 mapping can improve the accuracy of blood T1 values and can consequently increase the measurement accuracy of extracellular volume fraction. We speculate that these results may be related to the blood supply of both group tumors. Among our groups, the ccRCC group has the

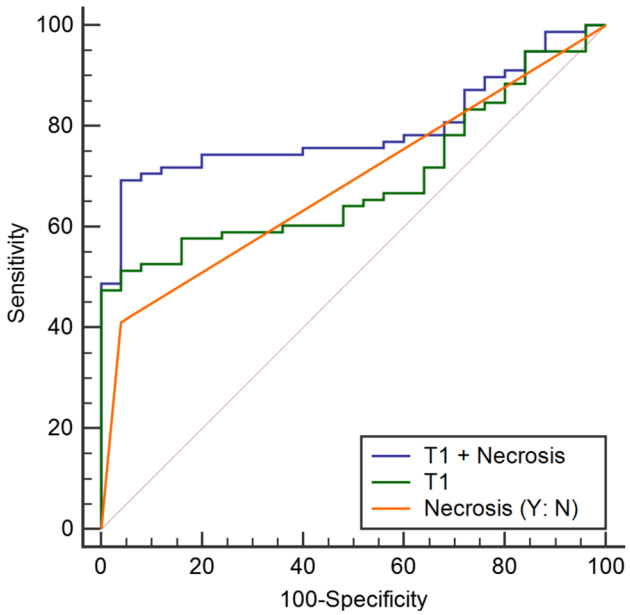

Fig. 4 Receiver operating characteristic (ROC) curve of significant parameter for differentiating benign from malignant renal tumor

highest percentage (61.5%) of malignant tumors, while pf-AMLs predominates (71.4%) in benign tumors. They all have a rich blood supply. This outcome may be more conducive to the clinical promotion of T1 mapping. Native T1 mapping can assist in detecting malignant renal tumors in patients with chronic kidney disease, thereby reducing the risk of adverse effects from contrast agents on renal function, as well as decreasing financial burdens [29].

Emerging evidence has begun to explore quantitative MRI biomarkers for renal mass characterization, with particular attention to the T1 mapping as a promising approach. Adams et al. [21] pioneered the application of this emerging quantitative MRI sequence in their prospective study of 27 ccRCC cases, demonstrating significant differences in post-contrast T1 reduction between low-grade (ISUP 1–2) and high-grade (ISUP 3–4) tumors ($p < 0.001$). While these initial findings highlighted T1 mapping's potential as an in vivo biomarker, the limited sample size ($n = 27$) and focus on larger tumors (mean diameter 6.35 ± 4.22 cm) left unanswered questions about its efficacy in small renal mass assessment. Subsequent work by Wang et al. [25] expanded this research to 56 renal tumors, including 40 ccRCCs and 16 angiomyolipomas (AMLs), revealing statistically significant differences in multiple T1-derived parameters (pre-/post-contrast T1 values, ΔT1, and T1 reduction ratios) between tumor types. However, their inclusion of 6 MRI-diagnosed AMLs without pathological confirmation and limited representation of sub-4 cm lesions (mean AML size 22.5 ± 9.7 mm). Our study specifically addresses these limitations by focused on solitary small renal masses (< 4 cm) that remain diagnostically challenging on conventional MRI, while incorporating both expanded sample size and comprehensive clinical-imaging correlation analysis. Emerging deep learning studies have systematically investigated the differentiation of small renal masses using multiphase contrast-enhanced CT, with best models achieving moderate diagnostic performance (AUC 0.80, 95% CI 0.75–0.85) in retrospective multicenter cohorts involving 1,703 histologically confirmed cases [30].

Additionally, our study demonstrates that tumor necrosis serves as an independent discriminative factor for SRMs. It's easy to understand. First, histopathologic analyses consistently link coagulative necrosis (CN) to aggressive tumor behavior, including higher ISUP nuclear grades, advanced pT stages, and metastatic potential [31, 32]. In ccRCC, CN correlate with a 5.27-fold increased risk of cancer-specific mortality compared to non-necrotic counterparts [31]. Second, Kuroe et al. [33] reported that tumors with dirty necrosis—characterized by neutrophilic infiltration and cellular debris—exhibit significantly shorter disease-free survival (HR 3.58, $p = 0.024$) and higher metastatic rates (40% vs. 13% in ghost necrosis) due to enhanced inflammatory microenvironment interactions. Finally, meta-analytic data confirm CN's independence from tumor size, as even subcentimeter necrotic lesions demonstrate a 1.37–1.55-fold increased risk of recurrence and mortality [32].

Moreover, several regular sequences for MRI inspection were analyzed in this study, such as the T2-weighted imaging and the strengthened formal of tumors, which have been proven to be helpful in the differentiation of benign from malignant tumors [19]. However, these characteristics were not independent influence factors for SRMs in our study. A meta-analysis by Shang et al. shows the sensitivity and specificity of routine MRI for the detection of small malignant masses achieved 0.85 (95% CI 0.79–0.90) and 0.83 (95% CI 0.67–0.92), respectively [34]. We consider that the reason may

be the advantage of a larger sample size for meta-analysis can't be ruled out. Furthermore, we excluded renal cysts and typical fat-containing renal lesions and included only solid tumors, which were difficult to make a definite diagnosis in the clinic. Thirdly, qualitative assessment based on the radiologist's decision might be inconsistent, especially when the sign was equivocal on the image [35]. This study hopes to be able to perform such assessments quantitatively and objectively.

This study still had some limitations. The first is the retrospective and single-center design of the study, which has certain limitations and may have retrospective bias. Second, we failed to conduct experiments to validate the relationship between T1 mapping and tumor pathophysiological changes [36]. Third, we just simply divided the SRMs into benign and malignant groups. However, large discrepancies in imaging manifestation exist between different tumor types, such as the discrepancy of ccRCC and papillary cancer in the malignant group, and oncocytoma and fp-AML in the benign group. Fourth, although we increased the sample size, more validations using a large sample size are still required to be confirmed. Fifth, there is no unified calculating parameter on T1 mapping. Therefore, a collaborative infrastructure development for multicenter studies is needed, so that the performance of T1 mapping techniques at different magnetic field strengths can be evaluated, and the histopathology of SRM types can be comprehensively studied.

5 Conclusions

Quantitative T1 mapping may be a promising noninvasive marker for classifying benign and malignant small renal tumors.

Acknowledgements Not applicable.

Lianting Zhong was listed as the first author. Danlan Lian and Ying Zhang have the same contribution to the conception and design of this manuscript. As a result, they are listed as co-first authors of this article. Jianjun Zhou and Xiaobo Qu have the same contribution to the design and guidance of this manuscript. As a result, they are listed as co-corresponding authors of this article.

Author contributions Xiao-Bo Qu participated in designing the study. Jian-Jun Zhou conceived and designed the study. Lian-Ting Zhong performed the study, collected data, and wrote the main manuscript text. Dan-Lan Lian and Ying Zhang labeled the data. Yu-Qin Ding and Jie-Feng Guo created and trained the models. Wei-Feng Lin and Sheng-Xiang Rao tested the models, analyzed the results, and prepared figures. All authors reviewed and approved the manuscript.

Funding The study was supported by the National Natural Science Foundation of China (82202285) and the Guiding Project on Medical and Healthcare from Xiamen Municipal Science and Technology Bureau in2024 (3502Z20244ZD1127).

Data availability The datasets generated during the current study are not publicly available due to the national legislature on patient data, but are available from the corresponding author on reasonable request.

Declarations

Ethics approval and consent to participate The study was conducted in accordance with the Declaration of Helsinki. We obtained permission from The Ethics Committee of Fudan University Affiliated Zhongshan Hospital in Shanghai (China). Informed consent requirement was waived because of its retrospective nature.

Competing interests The authors declare no competing interests.

References

1. Jayson M, Sanders H. Increased incidence of serendipitously discovered renal cell carcinoma. Urology. 1998;51(2):203–5. https://doi.org/10.1016/s0090-4295(97)00506-2.
2. Wong M, Goggins WB, Yip B, Fung F, Leung C, Fang Y, Wong S, Ng CF. Incidence and mortality of kidney cancer: temporal patterns and global trends in 39 countries. Sci Rep-UK. 2017;7(1):15698. https://doi.org/10.1038/s41598-017-15922-4.

3. Schieda N, Krishna S, Pedrosa I, Kaffenberger SD, Davenport MS, Silverman SG. Active surveillance of renal masses: the role of radiology. Radiology. 2022;302(1):11–24. https://doi.org/10.1148/radiol.2021204227.
4. Jeon HG, Lee SR, Kim KH, Oh YT, Cho NH, Rha KH, Yang SC, Han WK. Benign lesions after partial nephrectomy for presumed renal cell carcinoma in masses 4 cm or less: prevalence and predictors in Korean patients. Urology. 2010;76(3):574–9. https://doi.org/10.1016/j.urology.2009.11.082.
5. Remzi M, Ozsoy M, Klingler HC, Susani M, Waldert M, Seitz C, Schmidbauer J, Marberger M. Are small renal tumors harmless? Analysis of histopathological features according to tumors 4 cm or less in diameter. J Urology. 2006;176(3):896–9. https://doi.org/10.1016/j.juro.2006.04.047.
6. Fujii Y. Benign lesions at surgery for presumed renal cell carcinoma: an Asian perspective. Int J Urol. 2010;17(6):500. https://doi.org/10.1111/j.1442-2042.2010.02536.x.
7. Johnson DC, Vukina J, Smith AB, Meyer AM, Wheeler SB, Kuo TM, Tan HJ, Woods ME, Raynor MC, Wallen EM, Pruthi RS, Nielsen ME. Preoperatively misclassified, surgically removed benign renal masses: a systematic review of surgical series and United States population level burden estimate. J Urology. 2015;193(1):30–5. https://doi.org/10.1016/j.juro.2014.07.102.
8. Frank I, Blute ML, Cheville JC, Lohse CM, Weaver AL, Zincke H. Solid renal tumors: an analysis of pathological features related to tumor size. J Urology. 2003;170(6 Pt 1):2217–20. https://doi.org/10.1097/01.ju.0000095475.12515.5e.
9. Jewett MA, Mattar K, Basiuk J, Morash CG, Pautler SE, Siemens DR, Tanguay S, Rendon RA, Gleave ME, Drachenberg DE, Chow R, Chung H, Chin JL, Fleshner NE, Evans AJ, Gallie BL, Haider MA, Kachura JR, Kurban G, Fernandes K, Finelli A. Active surveillance of small renal masses: progression patterns of early stage kidney cancer. Eur Urol. 2011;60(1):39–44. https://doi.org/10.1016/j.eururo.2011.03.030.
10. Ray S, Cheaib JG, Pierorazio PM. Active surveillance for small renal masses. Rev Urol. 2020;22(1):9–16.
11. Halverson SJ, Kunju LP, Bhalla R, Gadzinski AJ, Alderman M, Miller DC, Montgomery JS, Weizer AZ, Wu A, Hafez KS, Wolf JJ. Accuracy of determining small renal mass management with risk stratified biopsies: confirmation by final pathology. J Urology. 2013;189(2):441–6. https://doi.org/10.1016/j.juro.2012.09.032.
12. McEachen JC, Leng S, Atwell TD, Tollefson MK, Friese JL, Wang Z, Murad MH, Schmit GD. Percutaneous renal tumor ablation: radiation exposure during cryoablation and radiofrequency ablation. Cardiovasc Inter Rad. 2016;39(2):233–8. https://doi.org/10.1007/s00270-015-1169-1.
13. Volpe A, Mattar K, Finelli A, Kachura JR, Evans AJ, Geddie WR, Jewett MA. Contemporary results of percutaneous biopsy of 100 small renal masses: a single center experience. J Urol. 2008;180(6):2333–7. https://doi.org/10.1016/j.juro.2008.08.014.
14. Jiang SH, Karpe KM, Talaulikar GS. Safety and predictors of complications of renal biopsy in the outpatient setting. Clin Nephrol. 2011;76(6):464–9. https://doi.org/10.5414/cn107128.
15. Patel HD, Johnson MH, Pierorazio PM, Sozio SM, Sharma R, Iyoha E, Bass EB, Allaf ME. Diagnostic accuracy and risks of biopsy in the diagnosis of a renal mass suspicious for localized renal cell carcinoma: systematic review of the literature. J Urol. 2016;195(5):1340–7. https://doi.org/10.1016/j.juro.2015.11.029.
16. Pedrosa I, Cadeddu JA. How we do it: managing the indeterminate renal mass with the MRI clear cell likelihood score. Radiology. 2022;302(2):256–69. https://doi.org/10.1148/radiol.210034.
17. Sankineni S, Brown A, Cieciera M, Choyke PL, Turkbey B. Imaging of renal cell carcinoma. Urol Oncol-Semin ORI. 2016;34(3):147–55. https://doi.org/10.1016/j.urolonc.2015.05.020.
18. Kang SK, Huang WC, Pandharipande PV, Chandarana H. Solid renal masses: what the numbers tell us. Am J Roentgenol. 2014;202(6):1196–206. https://doi.org/10.2214/AJR.14.12502.
19. Kay FU, Canvasser NE, Xi Y, Pinho DF, Costa DN, Diaz DLA, Khatri G, Leyendecker JR, Yokoo T, Lay AH, Kavoussi N, Koseoglu E, Cadeddu JA, Pedrosa I. Diagnostic performance and interreader agreement of a standardized MR imaging approach in the prediction of small renal mass histology. Radiology. 2018;287(2):543–53. https://doi.org/10.1148/radiol.2018171557.
20. Hectors SJ, Garteiser P, Doblas S, Page G, Van Beers BE, Waterton JC, Bane O. MRI mapping of renal T1: basic concept. Methods Mol Biol. 2021;2216:157–69. https://doi.org/10.1007/978-1-0716-0978-1_9.
21. Adams LC, Jurmeister P, Ralla B, Bressem KK, Fahlenkamp UL, Engel G, Siepmann S, Wagner M, Hamm B, Busch J, Makowski MR. Assessment of the extracellular volume fraction for the grading of clear cell renal cell carcinoma: first results and histopathological findings. Eur Radiol. 2019;29(11):5832–43. https://doi.org/10.1007/s00330-019-06087-x.
22. Jiang K, Ponzo TA, Tang H, Mishra PK, Macura SI, Lerman LO. Multiparametric MRI detects longitudinal evolution of folic acid-induced nephropathy in mice. Am J Physiol-Renal. 2018;315(5):F1252–60. https://doi.org/10.1152/ajprenal.00128.2018.
23. Tewes S, Gueler F, Chen R, Gutberlet M, Jang MS, Meier M, Mengel M, Hartung D, Wacker F, Rong S, Hueper K. Functional MRI for characterization of renal perfusion impairment and edema formation due to acute kidney injury in different mouse strains. PLoS ONE. 2017;12(3): e173248. https://doi.org/10.1371/journal.pone.0173248.
24. de Bazelaire CM, Duhamel GD, Rofsky NM, Alsop DC. MR imaging relaxation times of abdominal and pelvic tissues measured in vivo at 3.0 T: preliminary results. Radiology. 2004;230(3):652–9. https://doi.org/10.1148/radiol.2303021331.
25. Wang S, Li J, Zhu D, Hua T, Zhao B. Contrast-enhanced magnetic resonance (MR) T1 mapping with low-dose gadolinium-diethylenetriamine pentaacetic acid (Gd-DTPA) is promising in identifying clear cell renal cell carcinoma histopathological grade and differentiating fat-poor angiomyolipoma. Quant Imag Med Surg. 2020;10(5):988–98. https://doi.org/10.21037/qims-19-723.
26. Rossi SH, Klatte T, Usher-Smith J, Stewart GD. Epidemiology and screening for renal cancer. World J Urol. 2018;36(9):1341–53. https://doi.org/10.1007/s00345-018-2286-7.
27. Delahunt B, McKenney JK, Lohse CM, Leibovich BC, Thompson RH, Boorjian SA, Cheville JC. A novel grading system for clear cell renal cell carcinoma incorporating tumor necrosis. Am J Surg Pathol. 2013;37(3):311–22. https://doi.org/10.1097/PAS.0b013e318270f71c.
28. Robbers LF, Baars EN, Brouwer WP, Beek AM, Hofman MB, Niessen HW, van Rossum AC, Marcu CB. T1 mapping shows increased extracellular matrix size in the myocardium due to amyloid depositions. Circ Cardiovasc Imag. 2012;5(3):423–6. https://doi.org/10.1161/CIRCIMAGING.112.973438.
29. Rankin AJ, Mayne K, Allwood-Spiers S, Hall BP, Roditi G, Gillis KA, Mark PB. Will advances in functional renal magnetic resonance imaging translate to the nephrology clinic? Nephrology. 2022;27(3):223–30. https://doi.org/10.1111/nep.13985.

30. Dai C, Xiong Y, Zhu P, Yao L, Lin J, Yao J, Zhang X, Huang R, Wang R, Hou J, Wang K, Shi Z, Chen F, Guo J, Zeng M, Zhou J, Wang S. Deep learning assessment of small renal masses at contrast-enhanced multiphase CT. Radiology. 2024;311(2): e232178. https://doi.org/10.1148/radiol.232178.
31. Xu K, Liu L, Li W, Sun X, Shen T, Pan F, Jiang Y, Guo Y, Ding L, Zhang M. CT-based radiomics signature for preoperative prediction of coagulative necrosis in clear cell renal cell carcinoma. Korean J Radiol. 2020;21(6):670. https://doi.org/10.3348/kjr.2019.0607.
32. Zhang L, Zha Z, Qu W, Zhao H, Yuan J, Feng Y, Wu B. Tumor necrosis as a prognostic variable for the clinical outcome in patients with renal cell carcinoma: a systematic review and meta-analysis. BMC Cancer. 2018;18(1):870. https://doi.org/10.1186/s12885-018-4773-z.
33. Kuroe T, Watanabe R, Kojima M, Morisue R, Sugano M, Kuwata T, Masuda H, Kusuhara S, Matsubara N, Oda S, Ushiku T, Ishii G. Evaluation of the morphological features and unfavorable prognostic impact of dirty necrosis in renal cell carcinoma. J Cancer Res Clin. 2021;147(4):1089–100. https://doi.org/10.1007/s00432-020-03505-2.
34. Shang W, Hong G, Li W. MRI for the detection of small malignant renal masses: a systematic review and meta-analysis. Front Oncol. 2023;13:1194128. https://doi.org/10.3389/fonc.2023.1194128.
35. Schieda N, Davenport MS, Silverman SG, Bagga B, Barkmeier D, Blank Z, Curci NE, Doshi AM, Downey RT, Edney E, Granader E, Gujrathi I, Hibbert RM, Hindman N, Walsh C, Ramsay T, Shinagare AB, Pedrosa I. Multicenter evaluation of multiparametric MRI clear cell likelihood scores in solid indeterminate small renal masses. Radiology. 2022;303(3):590–9. https://doi.org/10.1148/radiol.211680.
36. Bardach C, Morski L, Mascherbauer K, Dona C, Koschutnik M, Halavina K, Nitsche C, Beitzke D, Loewe C, Waldmann E, Trauner M, Mascherbauer J, Hengstenberg C, Kammerlander A. Comparison of hepatic tissue characterization between T1-mapping and non-contrast computed tomography. J Clin Med. 2022. https://doi.org/10.3390/jcm11102863.